Earthquake Geotechnical Engineering for Protection and Development of Environment and Constructions – Silvestri & Moraci (Eds)
© 2019 Associazione Geotecnica Italiana, Rome, Italy, ISBN 978-0-367-14328-2

Measuring the improvements in synthetic seismograms using four generations of velocity models

J.G. Anderson
Nevada Seismological Laboratory, University of Nevada, Reno, Nevada, USA

H. Kawase
Disaster Prevention Research Institute, Kyoto University, Kyoto, Japan

ABSTRACT: Our ultimate goal is to develop synthetic seismograms that outperform ground motion prediction equations through incorporation of the physics of wave propagation. The present model uses synthetic Green's functions generated for flat-layered geological structure. We test four generations of velocity models to generate synthetics for the M5.8 Fukushima-Hamadori earthquake of March 19, 2011. Velocity model VM1 is given by JIVSM for the hypocenter of the earthquake. VM2 is the same, but with a modified Q model. VM3 uses instead the JIVSM velocity model for each station, with the modified Q model. VM4 substitutes a shallow velocity structure based on inversion of H/V from weak motions in earthquakes. The average standard deviation of Fourier and pseudoacceleration response spectra improves modestly as the models advance from VM1 to VM4. The improvement is marked at some stations, but not at others. A future challenge is to understand the physics behind these trends.

1 INTRODUCTION

Seismic risk analysis requires hazard estimates in the form of hazard curves and, increasingly, appropriate seismograms that are compatible with specific earthquakes on identified faults that might affect the site. This paper focuses on development of realistic synthetic seismograms that can serve as alternatives to past records.

In the process of developing a model for synthetic seismograms for engineering applications, the first question is the selection of an appropriate velocity model. The SCEC Broadband Platform, as described by Goulet et al. (2015), used regional models - one for northern California, one for the Mojave Desert, one for elsewhere in southern California, and two models to represent different regions in Japan. This project evaluates the benefits of going beyond regional models for the purposes of generating synthetic seismograms in two-dimensional structures.

We went through a number of iterations and model improvements. At the end, we selected four representative models to illustrate the effects of differences in the model concept. The result informs the trade-off between gathering more information and the reduction of sigma that can result from obtaining that information.

2 PROCEDURE

2.1 *The earthquake*

This case study considers the M_W5.8 earthquake of March 19, 2011 (36.7837 N, 140.5715 E), in the region near the border between Fukushima and Ibaraki Prefectures . The focal mechanism of this event is normal faulting, on a fault with a southeast strike (141°) dipping to the southwest (48°). Figure 1 shows the location of the earthquake and it's aftershocks in eastern Japan, north of Tokyo. It was recorded by the Japanese K-NET and KiK-net strong motion

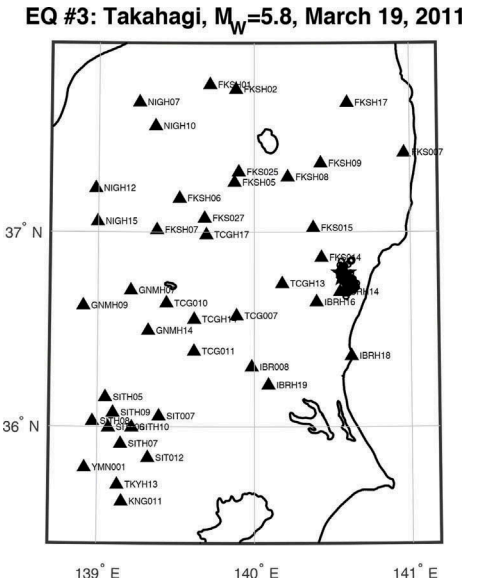

Figure 1. Locations of main shock, aftershocks, and stations.

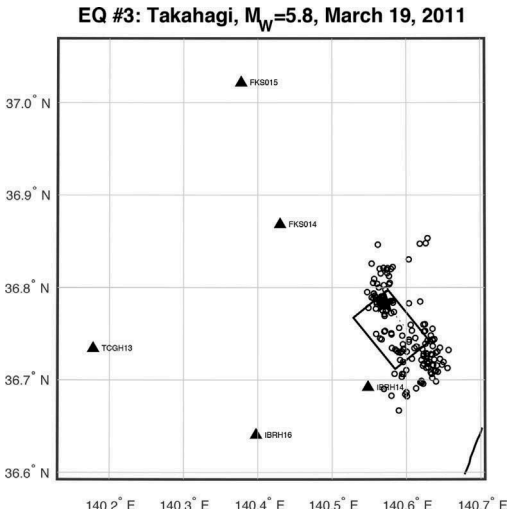

Figure 2. Details of the main shock, aftershocks, nearby stations, and the surface projection of the model fault plane.

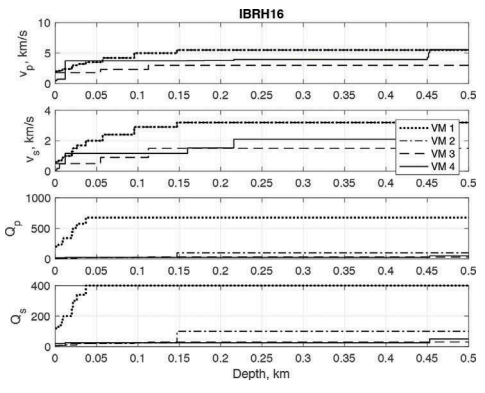

Figure 3. Velocity models at station IBRH16 compared to 0.5 km depth.

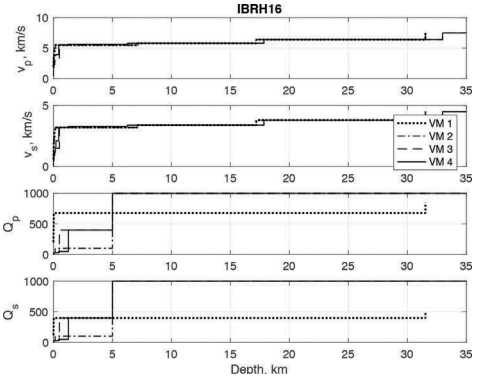

Figure 4. Velocity models at station IBRH16 compared to 35 km depth.

network. Figure 1 locates 42 stations within 200 km of the fault with estimated values of V_{S30}>500 m/s. These stations are used in this study.

2.2 *Synthetic seismograms*

This project aimed to reproduce key charancteristics of the records at all 42 stations through the use of the composite source model system of generating synthetic seismograms. This code has been described by Anderson (2015). Synthetics at all frequencies are generated using the representation theorem. This requires a slip model for the source, and Green's functions to transmit the effect of the source slip to the station. This study focuses on the velocity model used to calculate the Green's functions. However, an elementary review of the source model will be helpful.

The source model consists of the superposition of subevents, where each subevent is modeled as the source of a "Brune pulse" (Brune, 1970). Thus each subevent has a virtual radius, r_i, a time constant $\tau_i = r_i/(2.34\beta)$, and a time function $S(t) \sim \Delta\tau_s\, t \exp(-t/\tau)$. The pulse size is

normalized by a subevent stress drop, $\Delta\tau_s$ such that the time function integrates to the moment of a circular crack of that stress drop: $M_{0i} = (16/7)\Delta\tau_S\, r_i^3$ (Kanamori and Anderson, 1975). Each subevent has seismic magnitude $M_{Wi} = (2/3)(\log M_{0i} - 16.1)$ for moment in dyne-cm (Kanamori, 1977). The numbers and radii of subevents are chosen randomly from probability distributions that 1) satisfy a statistical Gutenberg-Richter relationship with b=1, and 2) sum to the target seismic moment of the earthquake. The largest allowed subevent has $r_{max} = W_E/4$ where W_E is the narrowest width of the fault. Subevents are placed on the fault at random, but a circle with radius r i cannot go outside of the fault limits. Each subevent starts at the time given by the distance from the hypocenter, divided by the rupture velocity. This model may break down for sites in the near field of the large subevents, but it generally seems to perform well. The total slip represented by the subevents, found by summing the virtual slip of all the subevents, results in variable slip on the fault. From this slip, it is possible to find the "strong motion generating area", and verify that it is consistent with the scaling of the Irikura recipe (Somerville et al., 1999). Furthermore, that slip distribution is consistent with the slip distribution reported by Thingbaijam and Mai (2016).

The Green's functions are all generated using a Fortran code first written by Y. Zeng, but subsequently modified, following the method described by Luco and Apsel (1983). This method represents the Earth with flat layers, where each layer is characterized by the thickness, P-wave and S-wave speeds, attenuation quality factors Qp and Qs, and density. This study considers the effectiveness of four approaches to determine the velocity model, as summarized in Table 1. Figures 3 and 4 illustrate the differences among the models for site IWTH16. The reasons for the change in the Q model will be pointed out in the discussion of the results.

3 RESULTS

It is useful to begin the discussion of the synthetics with images of selected synthetics, compared to data. For this purpose, this paper will focus on the station IBRH16. As seen on Figure 2, this station is located southwest of the fault, on the hanging wall side of the fault, but beyond the vertical projection of the fault to the surface. Figures 5, 6, and 7 compare the observed and one of the model set of synthetic acceleration, velocity, and displacements. For each station, synthetics were calculated for 50 realizations of the source. The synthetics for these figures were computed using VM4. The data and synthetics have similar amplitudes and durations for all three components of the ground motion. They also appear to have similar frequency content, although that is difficult to judge from looking at the time series.

Table 1. Velocity models used in this study.

Model	Source and Main Characteristics
VM 1	The velocity and Q model for the epicenter from JIVSM: http://www.jishin.go.jp/main/chousa/12_choshuki/dat/nankai/lp2012nankaie_ str.zip.
VM 2	Velocities are the same as VM1. Shallow Qp=Qs, as given by the procedure in Anderson (2015). Below 5 km, Qp=Qs=1000.
VM 3	Separate velocity model at each station location from JIVSM. Q is determined as in VM2.
VM 4	Modified from VM3, with shallow velocity from H/V ratios following Ducellier et al. (2013) and Nagashima et al. (2014).

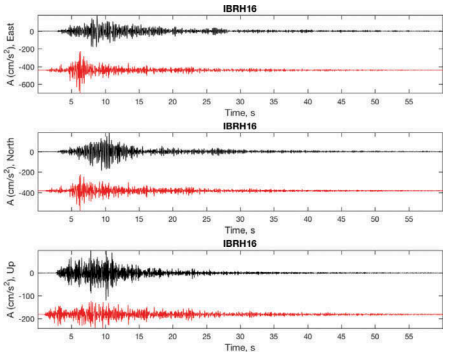

Figure 5. IBRH16 observed and sample synthetic accelerations using VM4.

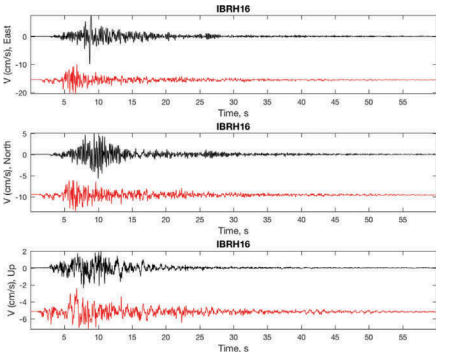

Figure 6. IBRH16 observed and sample synthetic velocities using VM4.

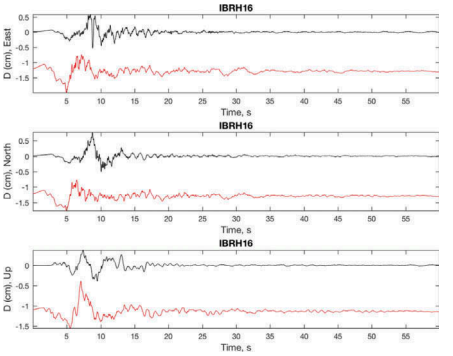

Figure 7. IBRH16 observed and sample synthetic displacements using VM4.

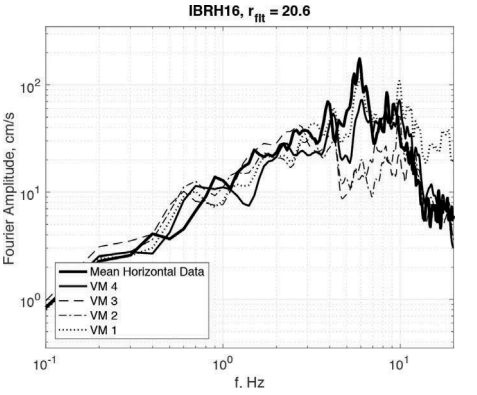

Figure 8. Observed Fourier amplitude spectra at IBRH16, and average predictions from each velocity model. These spectra have been smoothed, and show the amplitudes of the vector sum of the horizontal components.

Figure 8 compares the observed Fourier amplitude at station IBRH16 to the average, over 50 realizations, of the source for VM1, VM2, VM3, and VM4. Figure 9 shows the equivalent for the pseudo-spectral acceleration (PSA). As a quick visual impression, VM4 appears to have generated the most similar Fourier spectra, particularly at frequencies near the frequency where the data spectrum peaks. We attribute the approximate match in frequencies of spectral peaks at about 4 Hz, 6 Hz, and 8 Hz to the improvements in the velocity model based on the H/V. VM1 also shows a peak at 6 Hz, which we attribute to coincidence, as VM2 and VM3 are much smaller in this range, and their spectra do not match. The VM1 spectrum is too high from ~12–25 Hz, which we attribute to the Q model. This is one illustration of why the Q model needs to have very low values near the surface, as in Figure 4 and is used for VM2, VM3, and VM4. The broad trend of the model spectra below 4 Hz is the same, as should be expected, but none of these models have a convincing match of the finer structure in this frequency range.

Comparing the observed PSA spectrum with the four models (Figure 9), the result of VM4 seems to provide the best match. At long periods, all four spectra converge as expected. At the short period side of the spectrum, VM4 comes closest to predicting the observed peak acceleration. The width and amplitude of the VM4 model peak is closer to matching the data than

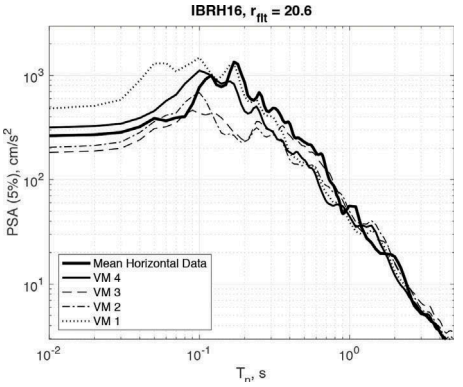

Figure 9. Equivalent of Figure 8 for the pseudo-acceleration response of data and average predictions.

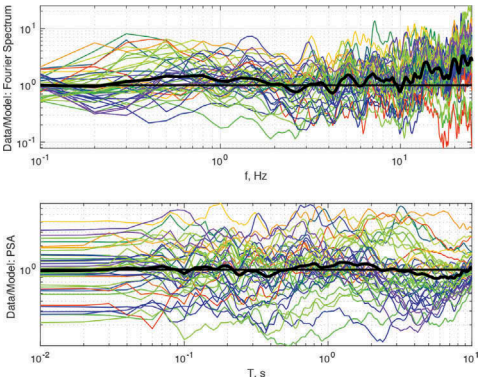

Figure 10. Average misfit, by station, of synthetic predictions from VM4. The line color follows the spectrum from red (nearest) to violet (farthest). The heavy black line is the 42 station average.

any of the others. VM2 and VM3 lack a peak in this period range. VM1 does have a peak that is similar to the data at Tn~0.2 s, but this model also has large peak between 0.05s and 0.1 s that is not present in the data.

Figure 10 shows the ratio of Data/Model for spectra such as those in Figures 8 and 9. This figure plots, on a logarithmic axis, the average spectral ratios for each of the 42 stations in Figure 1 based on the VM4 model as the denominator. For subsequent analysis, the residual is defined as the ln(data/model). At low frequencies/long periods, the residual converges to zero because that part of the spectrum is controlled by the seismic moment of the source. The subevent stress drop for each velocity model was adjusted to give zero residual for T_n=0. This is not necessarily the optimal choice, but is useful for the comparative purposes of this paper.

One test of the different velocity models is to see if there are trends in the residuals as a function of distance. Perusal of Figure 10 may show some trends, but it is easier to to see if spectral residuals at a specific frequency or period are plotted as a function of distance. This has been done, and Figure 11 shows the slopes, with their uncertainties, for each model at four frequencies. At 1 Hz and at ~3 Hz, the slopes are not zero, but a zero slope is within the one-sigma uncertainty range for all four models. At 10 Hz/0.1 s, the residuals in the slope is significantly non-zero for VM1, but not for the other three models. Again, this unacceptable feature has been corrected by the change in the attenuation structure illustrated in Figures 3 and 4. At the longest periods shown (0.3 Hz/3 s), all of the models have a significant tendency to have a larger residual at short distances, and a smaller residual at long distances.

Another way to compare the four velocity models is to compare the mean spectral residuals. This is shown in Figure 12. In this figure, the average response spectral period tends to be better for VM4 than any of the others. In the residuals for the Fourier spectrum, VM4 shows the largest deviation from 0.3–3 Hz, but tends to be better than the others at other frequencies. The corresponding standard deviations of the models, derived from the variability of station means as in Figure 10, is shown in Figure 13. Here, the differences seem small compared to the overall values. VM4 tends to be best from 1–10 Hz in the Fourier spectrum, and a corresponding period range in the response spectrum.

Figure 14 attempts to concisely summarize the observations in Figure 13. The misfit is the sum of the absolute values of the residuals in Figure 12, sampled on the log frequency/period axis scale. The standard deviation is the average of the standard deviations in Figure 13, sampled at equispaced points on the log frequency/period axis scale. The relative values of the standard deviations indicate that the Fourier amplitude models based on the apropriate deep structure beneath the site is better than a single regional model, and that incorporating

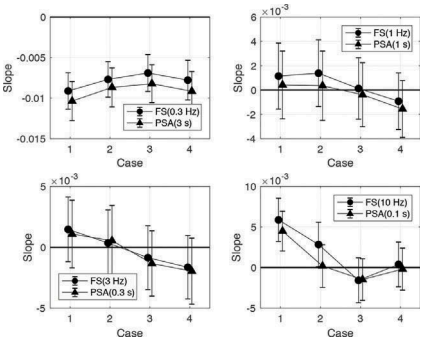

Figure 11. Residuals, by velocity model, as a function of distance at four different frequencies.

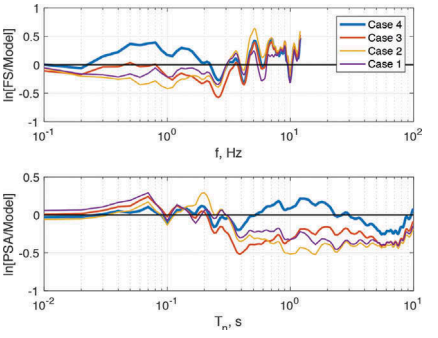

Figure 12. Mean residuals over 42 stations as a function of frequency for Fourier spectra (top) and by period for response spectra (bottom), by velocity model.

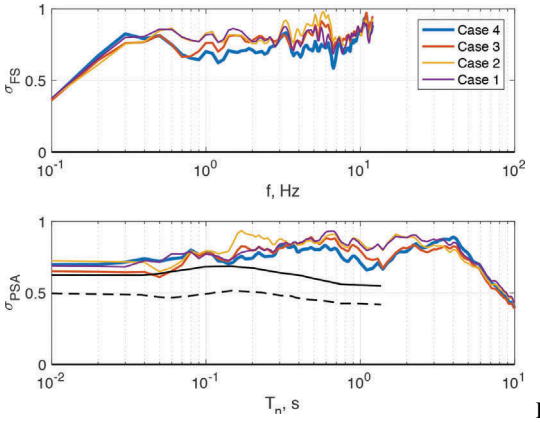

Figure 13. Standard deviation of residuals over 42 stations as a function of frequency for Fourier spectra (top) and by period for PSA (bottom), by velocity model. For PSA, the solid and dashed lines show values of φ and φ_{SS}, respectively the intraevent and single-station standard deviations measured at KiK-net stations by Rodriguez-Marek et al. (2011).

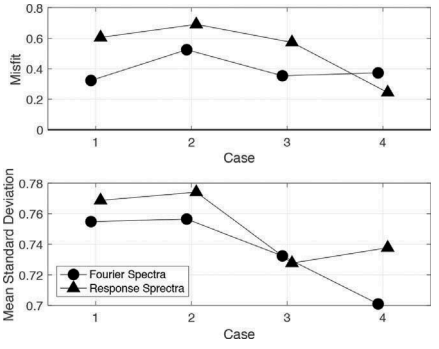

Figure 14. Effect of the velocity models on the mean standard deviation, the average over the spectrum of the standard deviations shown in Figure 13.

shallow site information is even better. The impact of including the shallow site information on the response spectrum does not show subsequent reduction of sigma.

4 DISCUSSION/CONCLUSIONS

There are situations where broadband synthetic seismograms that satisfy the wave equation are useful and flat-layered velocity models are available but three dimensional models are not yet available. There are also situations where broadband ground motions in flat-layered models are sufficient for addressing specific scientific questions. This case study is relevant to those situations.

The broadest conclusion is that on average, it seems better to use a velocity model that is appropriate for the site, including near-surface velocities, if that is available. In the best case, a set of site-specific models like those used for VM4 might, hopefully, provide ground motion estimates with uncertainties that are comparable to single-station sigma in ground motion prediction equations. Figure 13 shows, however, that the standard deviations found using the synthetics have standard deviations of their estimated parameters that are considerably greater than the single-station sigma values found by Rodriguez-Marek et al. (2011) at KiK-net stations. Consistent with this observation, review of spectra on a site-by-site basis finds that the extent to which the models were improved in the shift from VM3 to VM4 is variable. At the five nearest stations (Figure 2), mean residuals and standard deviations are generally comparable to the results in Figures 12 and 13. A future challenge is to understand why these results are mixed, and consider how they can be improved to close the gap between the best models of synthetic seismograms and the results for single-station sigma.

The selected station, IBRH16, was chosen primarily because of its location close to the fault off the hanging wall. Many urban areas near normal faults share that geometry. However, as a qualitative impression, in about a third of the cases, like IBRH16, VM4 was obviously best, in another third the spectral shapes were changed towards the observations and away from the other models, but the amplitude of the fit was off, and in about a third, model VM4 did not stand out from the other models. Indeed, it is clear in Figure 10 that there are some stations with conspicuously poor agreement with the model. We have observed, for instance, that some of the largest residuals are seen at stations in deep valleys near the west side of Honshu, within the volcanic range. It is known that Q is relatively low in that region (e.g. Nakano et al., 2016), and perhaps also topography has an effect. This is one example where the physics affecting the ground motions is incompletely modeled in this study.

Another shortcoming in the physics included in the flat-layered model is seen in Figure 11, which indicates that the low frequency surface waves are not attenuating fast enough, on average. Indeed, displacement seismograms at stations beyond 150 km show strong surface waves that are not present in the data, and their Fourier spectra show peaks at ~0.2 Hz that are stronger than the data, It seems likely that scattering by near-surface complexity, that is not represented in the model, would reduce the amplitude of these surface waves. The very low Qp and Qs in the near-suface layers apparently does not cause these waves to attenuate strongly enough. This might alternatively be corrected with a frequency-dependent Qp and Qs, but that is not currently implemented in the Green's function calculations. There are uncomplicated patches to the present model. We have experimented with separate Green's functions generated with low Q, and combining them with the high-frequencies of the models shown here using match filters. The three-dimensional finite difference or finite element calculations also have the capability to model these low frequencies well, in those few regions where the velocity model is extremely well known. Nonetheless, this effect seems to indicate that special attention is needed at large distances.

As a summary, we do see applications for synthetic seismograms generated in flat-layered velocity structures. This case study shows, based on a subset of sites in Tohoku with Vs30>500 m/s, both successes and opportunities for improvement. In this region with very complicated geology, the simple approximation of using a separate velocity structure appropriate for each site results in improvements in the standard deviations of the predictions compared to using a single regional velocity model. Detailed site-specific models of the shallow geological structure brought mixed success and a modest reduction of the standard deviation.

ACKNOWLEDGEMENTS

John Anderson thanks the Disaster Prevention Research Institute of Kyoto University for the opportunity to visit Kyoto as a Visiting Professor in 2018.

REFERENCES

Anderson, J.G. 2015. The composite source model for broadband simulations of strong ground motions. *Seism. Res. Lett*. 86: 68–74.

Anderson, J.G., R.J. Brune, J.N. Brune & G.P. Biasi 2017. Wave propagation and source models for synthetic seismograms compatible with strong motion applications, *Proceedings, 16th World Conference on Earthquake Engineering*, Santiago, Chile, January 9–13, 2017: Paper No. 4023.

Brune, J.N. 1970. Tectonic Stress and the Spectra of Seismic Shear Waves from Earthquakes, *J. Geophys. Res*. 75: 4997–5009.

Ducellier, A., H. Kawase & S. Matsushima 2013. Validation of a new velocity structure inversion method based on horizontal-to-vertical (H/V) spectral ratios of earthquake motions in the Tohoku area, Japan, *Bull. Seism. Soc. Am*. 103 (2A): 958–970.

Goulet, C.A., N.A. Abrahamson, P.G. Somerville & K.E. Wooddell 2015. The SCEC Broadband Platform validation exercise: methodology for code validation in the context of seismic-hazard analyses, *Seism. Res. Lett*. 86: 17–26.

Kanamori, H. 1977. The energy release in great earthquakes, *J. Geophys. Res*. 82, 2981–2987.

Kanamori, H. & D.L. Anderson 1975. Theoretical basis of some empirical relations in seismology, *Bull. Seism. Soc. Am*. 65: 1073–1095.

Nagashima, F., S. Matsushima, H. Kawase, F.J. Sánchez-Sesma, T. Hayakawa, T. Satoh & M. Oshima 2014. Application of Horizontal-to-Vertical (H/V) Spectral Ratios of Earthquake Ground Motions to Identify Subsurface Structures at and around the K-NET Site in Tohoku, Japan, *Bull. Seism. Soc. Am*. 104: 2288–2302.

Nakano, K., S. Matsushima & H. Kawase 2016. Statistical properties of strong ground motions from the generalized spectral inversion of data observed by K-NET, KiK-net, and the JMA Shindokei Network in Japan, *Bull. Seism. Soc. Am*. 105: 2662–2680.

Luco, J.E. & R.J. Apsel 1983. On the Green's function for a layered half-space, part I, *Bull. Seism. Soc. Am*. 73: 909–929.

Rodriguez-Marek, A., G.A. Montalva, F. Cotton & F. Bonilla 2011. Aznalysis of single-station standard deviation using the KiK-net data, *Bull. Seism. Soc. Am*. 101: 1242–1258.

Somerville, P., K. Irikura, R. Graves, S. Sawada, D. Wald, N. Abrahamson, Y. Iwasaki, T. Kagawa, N. Smith & A. Kowada 1999. Characterizing crustal earthquake slip models for the prediction of strong ground motion, *Seism. Res. Lett*. 70: 59–80.

Thingbaijam, K.K.S. & P.M. Mai 2016. Evidence for truncated exponential probability distribution of earthquake slip, *Bull. Seism. Soc. Am*. 106: 1802–1816.